

Sliding Mode Control based MPPT and Output Voltage Regulation of a Two-stage Stand-alone PV System

Nelson Luis Manuel (✉ nelsonluismanuel@gmail.com)

Kırıkkale Üniversitesi <https://orcid.org/0000-0002-7217-3387>

Nihat İnanç

Kırıkkale Üniversitesi: Kırıkkale Üniversitesi

Research Article

Keywords: PV Systems, MPPT, Voltage Regulation, Sliding Mode Control, APF-P&O

Posted Date: June 27th, 2022

DOI: <https://doi.org/10.21203/rs.3.rs-1612537/v1>

License:   This work is licensed under a Creative Commons Attribution 4.0 International License.

[Read Full License](#)

Version of Record: A version of this preprint was published at Power Electronics and Drives on August 30th, 2022. See the published version at <https://doi.org/10.2478/pead-2022-0012>.

Sliding Mode Control based MPPT and Output Voltage Regulation of a Two-stage Stand-alone PV System

Nelson Luis Manuel^{1*†} and Nihat İnanç^{1†}

¹Department of Electrical and Electronics Engineering, Kırıkkale University, Yahşihan, 71450, Kırıkkale, Turkey.

*Corresponding author(s). E-mail(s): nelsonluismanuel@gmail.com;

†These authors contributed equally to this work.

Abstract

When it comes to reducing emissions caused by the generation of electricity through conventional sources, among different renewable energies, the solar gains prominence, due to its geographical availability, simplicity of implementation and absence of moving parts. However, the performance of photovoltaic systems is dependent on environmental conditions. Depending on temperature and solar irradiation, the PV system has an operating point where maximum power can be generated. The techniques that are implemented to find this operating point are the so-called maximum power point tracking (MPPT) algorithms. Since weather conditions are variable in nature, the output voltage of the PV system needs to be regulated to remain equal to the reference. Most of the existing studies focus either on MPPT or on voltage regulation of the PV system. In this paper, the two-stage PV system is implemented so that both MPPT and voltage regulation are achieved simultaneously. Additionally, an improved version of the Perturb and Observe (P&O) algorithm based on artificial potential fields (APF), called APF-P&O, is proposed. Sliding Mode Controllers with appropriate control laws are designed for both stages of conversion. Simulations performed in MATLAB/Simulink software prove the superiority of the proposed APF-P&O method over the conventional P&O method in terms of convergence time, output power ripples and sensitivity to step sizes. At the same time, the voltage regulation issue is also solved, where the output voltage is fixed to the value of 32 V, regardless of variations in solar irradiation.

Keywords: PV Systems, MPPT, Voltage Regulation, Sliding Mode Control, APF-P&O

1 Introduction

In order to ensure a sustainable future, many countries have been devising various strategies. In the context of energy systems, one of these strategies is the reduction or replacement of electricity generation based on non-renewable energies through the implementation of energy generation systems based on sources that are environmentally friendly. Solar energy, among other forms of

renewable energy, has been gaining both scientific and industrial interest in recent years due to its wide availability [1]. The application of photovoltaic systems in distributed generation and DC microgrids, not to mention the development of power electronics technology, further extend the facets of research on solar energy. However, the efficiency of a photovoltaic system is highly dependent on environmental conditions. Furthermore, for the generated power to be of high quality,

the voltage delivered by the PV system needs to be regulated. Therefore, to increase the efficiency of the photovoltaic system and guarantee high quality of the energy produced, it is necessary to implement strategies to track the point of maximum power and regulate the output voltage.

State-of-the-art studies and comparison of different methods for MPPT are carried out in [2]–[4]. Among different techniques, Perturb and Observe (P&O) and Incremental Conductance (InC) are commonly used for MPPT due to their easy implementation [5]. Some variants of these algorithms have been reported to improve the settling time and reduce output power fluctuations of the PV system. In order to overcome the drawbacks of the conventional P&O, an adaptive P&O method based on the Manhattan metric distance is proposed in [6]. An MPPT technique is proposed in [7], where the InC method is used to improve the convergence speed and the particle swarm optimization (PSO) algorithm is used to reduce ripples in the output power of a PV system. A hybrid technique for MPPT that combines a modified version of P&O and the chimp optimization algorithm (ChOA) is proposed in [8]. The Owl search algorithm is used together with the InC method to reduce the convergence time to the maximum power point and mitigate the inherent limitations of the conventional InC method in [9]. An improved version of the InC and integral regulator (IR) is used to track the peak output power of a PV system interfaced by a DC-DC boost converter in [10]. In [11], the Roach Infestation (RI) algorithm is presented for the MPPT of a photovoltaic system, and fuzzy logic is used to generate variable step sizes for the InC method in [12].

Different approaches to voltage regulation can also be found in the literature, including the classic PID Control [13], feedback linearization [14], Fuzzy Logic Control [15], Model Predictive Control [16], Sliding Mode Control [17], among others. Sliding Mode Control (SMC) has been reported as a convenient technique for controlling the voltage of DC-DC converters, since its operating structure is inherently commutative [18].

Many of the studies presented in the literature separately address the maximum power tracking and voltage regulation strategies for PV systems, instead of dealing with both at the same time [19]. However, for the delivered power to have a high

quality and to improve the efficiency of the photovoltaic system, both the MPPT and voltage regulation are aspects that must be taken into account simultaneously. To satisfy both objectives, the two-stage conversion topology is employed to control the photovoltaic system [20].

Therefore, in this paper the two-stage PV system control for maximum power point tracking and voltage regulation is presented. In the first stage, the boost converter is used and an improved version of P&O is proposed to find the PV voltage corresponding to the maximum power point. The reference voltage found by the P&O serves as an input to the Sliding Mode Controller, which then sends the necessary control signals to the boost converter so that maximum power is generated. In the second stage, the buck converter is used for voltage regulation and its control is done by applying a Sliding Mode Controller. In this manner, both MPPT and voltage regulation issues are simultaneously addressed.

2 Structure of the Photovoltaic System

The structure of a photovoltaic system can be separated into two essential parts: the photovoltaic module and the conversion subsystem [1]. The PV system studied in this paper is based on the two-stage conversion topology, as illustrated in Figure 1. The first DC-DC converter is a step-up (or boost) and the second one is a step-down (or buck) converter. The boost converter is used to modify the output impedance seen from the photovoltaic module terminals so that the point of intersection between the I-V characteristic curve of the PV module and the load line matches the point of maximum power that can be delivered under the given environmental conditions. In the second stage, the stability of the voltage supplied to the loads is achieved through the control of the step-down converter.

2.1 Electrical circuit of a Photovoltaic Cell

The photovoltaic cell is considered as the basic constituent of a PV module [21]. The PV cells are electrically connected in series and/or parallel to achieve the voltage, current and power levels for which the module is designed [22]. The

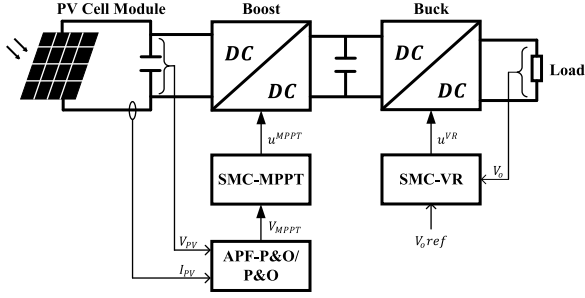


Fig. 1 Schematic of the applied control strategy for the two-stage PV system.

power delivered by the photovoltaic generator is dependent on the ambient temperature and solar irradiation. Generally, to model the behavior of a photovoltaic cell, an electrical circuit composed of a current source (I_{ph}), a diode (D), a series resistance (R_s), and a parallel resistance (R_{sh}), is considered. The resistance R_{sh} is connected in parallel with an inverted diode D to express non-linearity and losses due to leakage currents, and resistance R_s is used to model voltage drops when the module is connected to load [21]. The electrical circuit of a photovoltaic cell is shown in Figure 2.

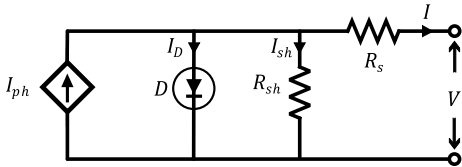


Fig. 2 Electrical circuit of a single diode PV cell.

Applying Kirchoff's current law to the electrical circuit of the single-diode photovoltaic cell model, the expression of the output current of the PV cell can be found as shown in Equation 1.

$$I = I_{ph} - I_D - I_{sh} \quad (1)$$

where I is the output current of the PV cell, I_{ph} is the photo-generated current, I_D is the current through the diode, and I_{sh} is the current through the resistor R_{sh} .

The expression to determine the current flowing through the diode, also known as a Shockley equation, can be computed using the Equation 2

[23].

$$I_D = I_o \left\{ \exp \left[\frac{q(V + IR_s)}{AkT} \right] - 1 \right\} \quad (2)$$

Therefore, the equation of the PV cell output current can be rewritten as in Equation 3.

$$I = I_{ph} - I_o \left\{ \exp \left[\frac{q(V + IR_s)}{AkT} \right] - 1 \right\} - \frac{(V + IR_s)}{R_{sh}} \quad (3)$$

where, I_o is the saturation current, q is the electron charge ($q = 1.6010^{-19}C$), k is the Boltzmann constant ($k = 1.3810^{-23}J/K$), T is the operating temperature of the cell, and A is the idealization constant of the diode D . The photo-generated current is dependent on temperature and solar irradiation. It is defined as demonstrated in Equation 4.

$$I_{ph} = [I_{scn} + k_i(T - T_n)] \frac{G}{G_n} \quad (4)$$

where I_{scn} denotes the short-circuit current under the standard test conditions ($T_n = 25^\circ C$ and $G_n = 1000W/m^2$), T is the ambient temperature, T_n is the nominal temperature, G and G_n are the actual and nominal irradiances, respectively, and k_i is the temperature coefficient of the short-circuit current. The saturation current of the photovoltaic cell is mathematically defined by Equation 5.

$$I_o = I_{rr} \left(\frac{T}{T_n} \right)^3 \exp \left[\frac{qE_g}{kA} \left(\frac{1}{T_n} - \frac{1}{T} \right) \right] \quad (5)$$

where I_{rr} is the reverse saturation current at temperature T_n and solar irradiation G_n , E_g is the band gap energy of the silicon PV cell ($E_g = 1.10eV$). The rest of the parameters remain with the same definitions previously made.

2.2 State-Space Averaged Models of the DC-DC Converters

In this subsection, the models of the DC-DC converters, which are part of the conversion circuit of the photovoltaic system under study, are presented. The DC-DC boost converter is used in the first stage of the conversion. This converter, in addition to boosting the output voltage

of the solar panel, is used to ensure that the power extracted from the PV module is the maximum possible by switching (ON and OFF) the input signal of the transistor Q at high frequencies. In Figure 3, the boost converter circuit is shown. Considering the continuous conduction

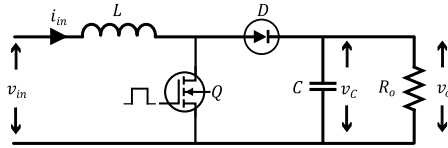


Fig. 3 Circuit of a DC-DC boost converter.

mode (CCM) of operation and choosing the current through the inductor and the voltage across the capacitor as the state variables, the averaged model of the boost converter can be defined by Equations (6) and (7) [24], [25].

$$\frac{di_L(t)}{dt} = -(1-u)\frac{1}{L}v_C(t) + \frac{1}{L}v_{in} \quad (6)$$

$$\frac{dv_C(t)}{dt} = (1-u)\frac{1}{C}i_L(t) - \frac{1}{RC}v_C(t) \quad (7)$$

where, i_L denotes the current through the inductor ($i_L = i_{in}$), v_C is the voltage across the capacitor ($v_C = v_o$), u is the control signal ($u \in \{0, 1\}$). In the boost converter circuit, the parameters R , L and C represent the load resistance, the input circuit inductance, and the output filter capacitance, respectively, and v_{in} is the supply voltage of the step-up converter.

For the second stage of conversion, the DC-DC buck converter is considered. Here, the buck converter is used to step down and stabilize the voltage delivered to the load. In Figure 4, the circuit of the buck-type DC-DC converter is shown. Considering that during the operation of the buck converter the average value of the current passing through the inductor does not reach zero, and adopting the current in the inductor and the capacitor voltage as the state variables, the averaged model of the buck converter is mathematically summarized by Equations (8) and (9).

$$\frac{di_L(t)}{dt} = -\frac{1}{L}v_C(t) + \frac{u}{L}v_{in} \quad (8)$$

$$\frac{dv_C(t)}{dt} = \frac{1}{C}i_L(t) - \frac{1}{RC}v_C(t) \quad (9)$$

where, i_L is the current through the inductor, v_C is the voltage across the capacitor ($v_C = v_o$), u is the control signal ($u \in \{0, 1\}$). In the buck converter circuit, the parameters R , L and C represent the load resistance, the circuit inductance, and the output filter capacitance, respectively, and v_{in} is the supply voltage of the step-down converter.

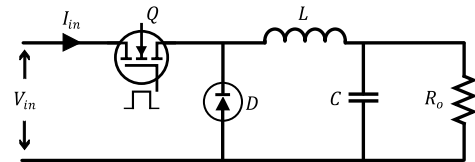


Fig. 4 Circuit of a DC-DC buck converter.

3 Control Strategy for MPPT

In order to get the best out of the solar generation system, tracking the maximum power point is crucial. There are several methods for Maximum Power Point Tracking. Among the different methods, the Perturb Observe is one of the most popular due to its simplicity [24]. Furthermore, in the P&O method, prior knowledge of the characteristics of the photovoltaic module is not required [22]. The operation of the P&O method is based on perturbing the output voltage of the PV module and observing the resultant output power. If the actual value of the measured power $P(k)$ is greater than its previously obtained value $P(k-1)$, then the direction of the perturbation is maintained, otherwise, the movement of the perturbation is done in the opposite direction [23]. In Figure 5, the flowchart that summarizes the operation of the P&O algorithm is depicted. As shown in the flowchart, the algorithm begins by sensing the values of voltage $V(k)$ and current $I(k)$ to compute the power $P(k)$ generated by the PV system. Then, the difference between the actual voltage value and its previous value $V(k-1)$ is computed and saved in the variable ΔV . The difference between the actual value of the measured power and its previous value $P(k-1)$ is also calculated and the result is recorded in the variable ΔP . Afterwards, the output voltage V of the photovoltaic system is perturbed (increases or decreases) depending on the ΔP and ΔV signals. The amount of increase or decrease of the output voltage is defined by the value ΔD . The value

ΔD is chosen based on tests and simulations [24]. If very small ΔD values are chosen, the system becomes slow to find the maximum power point, on the other hand, very large ΔD values can result in loss of information creating high levels of ripple in the generated power. Therefore, the trade-off between the time of convergence to the maximum power point and the steady-state ripple levels of the generated power must be taken into account when defining the value of ΔD .

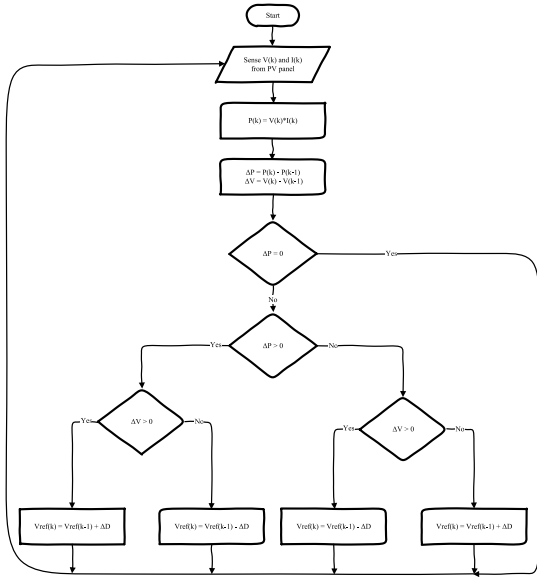


Fig. 5 Flowchart showing the operation of the P&O method.

3.1 Proposal for Improvement of the Conventional P&O Method

In this subsection, a proposal to improve the conventional P&O method is presented. The improvement is based on artificial potential fields (APF), hereinafter also referred to as APF-P&O. The proposed method, besides being simple to implement, has no computational complexity. Its implementation is done by adding just a few lines of code to the original method, and only depends on the output voltage of the photovoltaic module (which is already an input of the conventional P&O method), i.e., the proposed APF-P&O method does not increase the number of input variables of the conventional method. In APF, the target point or desired region is modeled as a point

or zone with an attractive potential field that pulls the controlled states towards the desired point or region [26]. Assuming that the minimum and maximum values of expected solar irradiation and the respective voltage values at the point of maximum power are known, a zone of attraction that contains all points of maximum power for the range of expected solar irradiation can be defined, as shown in Figure 6. The idea is to produce attractive forces so that the output voltages of the PV module remain in the attraction zone, which is the zone where the maximum power points are located. The attractive potential field

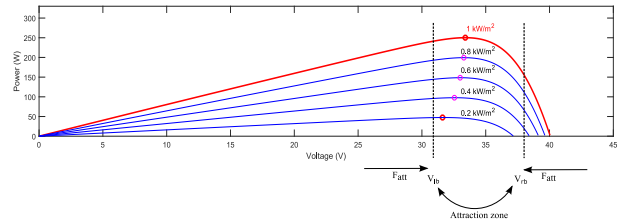


Fig. 6 Principle of the proposed APF-P&O method.

can be defined according to Equation (10), where $U_{att}(V_{PV})$ denotes the attractive potential field, K_{att} is a positive design constant, V_{PV} is the output voltage of the PV module, V_{lb} and V_{rb} are the left and right boundary voltages of the attraction zone, respectively.

$$U_{att}(V_{PV}) = \begin{cases} \frac{1}{2}K_{att}(V_{PV} - V_{lb})^2, & V_{PV} < V_{lb} \\ \frac{1}{2}K_{att}(V_{PV} - V_{rb})^2, & V_{PV} > V_{rb} \end{cases} \quad (10)$$

Applying the negative gradient to the attractive field expression, the corresponding attractive force is obtained, as shown in Equation (11).

$$F_{att} = -\nabla(U_{att}) = \begin{cases} K_{att}(V_{lb} - V_{PV}), & V_{PV} < V_{lb} \\ K_{att}(V_{rb} - V_{PV}), & V_{PV} > V_{rb} \end{cases} \quad (11)$$

where F is the resultant force of attraction. The law to determine the step size for the proposed APF-P&O algorithm is established according to

Equation (12).

$$\Delta D = \begin{cases} \chi, & V_{lb} \leq V_{PV} \leq V_{rb} \\ F_{att}, & otherwise \end{cases} \quad (12)$$

where χ is a relatively small positive design parameter that represents the step size when the algorithm is in the attraction zone. The value of χ is set small to reduce steady-state power fluctuations. As can be noticed, while the voltage generated by the PV system is outside the attraction zone, the algorithm generates forces of attraction necessary to bring the voltage to the zone where the maximum power points are located, and thus the convergence speed is increased.

3.2 Sliding Mode Controller for MPPT

The voltage at the maximum power point (V_{MPP}) estimated by the P&O method or by the proposed APF-P&O serves as a reference for the Sliding Mode Controller (SMC). The implemented SMC will produce the necessary control signals to make the output voltage of the PV module equal to the reference voltage, thus reaching the maximum power point (MPP). Assuming the error (e) as the difference between the PV module output voltage (V_{PV}) and the reference voltage (V_{MPP}), a sliding surface s can be defined as in Equation (13).

$$s = e = V_{PV} - V_{MPP} \quad (13)$$

The SMC control law u to achieve the MPPT can be defined as in Equation (14).

$$u = \frac{1}{2} [1 + \text{sign}(s)] \quad (14)$$

A rigorous stability analysis is presented in section 3 of the paper [24], where it is demonstrated that, in fact, by applying this control strategy, the system stability conditions at the MPP of the PV module interfaced with a boost converter are satisfied.

4 Control Strategy for Output Voltage Regulation

In this section, our attention is devoted to the strategy applied for the regulation of the output voltage of the photovoltaic system. Sliding

Mode Controller has been recognized as one of the powerful control strategies for power converters [27]. SMC is a robust non-linear control technique, which uses a discontinuous control action that switches between two different system structures, in such a manner that a new system motion, known as sliding mode, is achieved on a surface (or manifold) previously designed for this end [28]. This characteristic of switching between different structures of the system, makes the SMC a convenient control technique to be applied in DC-DC power converters, which are switching devices by their nature [18]. For these reasons, the SMC is chosen for the regulation of the output voltage of the PV system. In the following subsections, details about the technique used are presented.

4.1 Sliding Mode Controller Design for Output Voltage Regulation

One of the important features of the Sliding Mode Control is its low sensitivity to system parameter variations [29]. This is possible by employing a high-switching control law, which forces the system trajectories to converge in a predetermined zone within the state space and to remain in this zone thereafter. In SMC parlance, this zone is denoted as a sliding surface. Considering the buck converter state-space model presented earlier, the sliding surface is defined as in Equation (15) [30].

$$\sigma(x) = x_1 - x_1^*; \quad x_1^* = \mu_1 (x_2 - x_2^*) + \mu_2 \int (x_2 - x_2^*) \quad (15)$$

where $\sigma(x)$ is the sliding surface, x_1 is the current through the inductor, x_2 denotes the voltage across the capacitor, μ_1 and μ_2 are design parameters, x_1^* is the desired current, x_2^* is the desired voltage, and R denotes load resistance. The control objective is to make the output voltage x_2 of the PV system equal to the desired voltage x_2^* . This problem can also be redefined in terms of the current through the inductor, i.e., a control law u should be found such that the current x_1 is equal to its reference value x_1^* . If this occurs, then the difference $\Delta x_2 = x_2^* - x_2$, which leads to $\Delta \dot{x}_2 = -(1/RC)\Delta x_2$, will tend to zero over time [18]. In this paper, the cascade control structure of the SMC is adopted, where the inner loop current reference is obtained from the outer loop

voltage control using a linear controller [28]. In order to drive the system state variables to the sliding surface ($\sigma = 0$), the control law u presented in Equation (16) is employed [18].

$$u = \frac{1}{2} [1 - \text{sign}(\sigma)] \quad (16)$$

The stability analysis of the system applying the defined control law can be done using Lyapunov's theory. In Equation (17), the Lyapunov function $V(\sigma)$ that will be considered to evaluate the stability is presented .

$$V(\sigma) = \frac{1}{2} \sigma^2 \quad (17)$$

For the system to be considered stable, the selected Lyapunov function has to meet the following conditions [29] :

- $V(\sigma) > 0$;
- $V(\sigma) = 0 \Leftrightarrow \sigma = 0$;
- $\dot{V}(\sigma) = \sigma \dot{\sigma} < 0$.

It is simple to conclude that the first two conditions are fulfilled by the selected function, except for the third condition which deserves demonstration. The third condition is also known as the reaching condition in the Sliding Mode Control literature. Computing the derivative of the sliding surface presented in Equation (15), Equation (18) is obtained.

$$\dot{\sigma} = \dot{x}_1 = \left(\frac{v_{in}}{L} u - \frac{1}{L} x_2 \right) \quad (18)$$

If $\sigma < 0$, then $u = 1$. From Equation 18, in order for $\dot{\sigma} > 0$ to be satisfied, the output voltage has to be positive (i.e. $x_2 > 0$). Similarly, if $\sigma > 0$, then $u = 0$. For $\dot{\sigma} < 0$ to be satisfied, the output voltage has to be less than the input voltage (i.e. $x_2 < v_{in}$). In other words, the reaching condition will be fulfilled as long as the condition ($0 < x_2 < v_{in}$) is satisfied. In the case of buck converter, this condition is inherently accomplished. Therefore, it can be concluded that applying the presented control law, the stability of the system will be achieved [31]. The strategy implemented to regulate the voltage of the photovoltaic system is summarized in Figure 7.

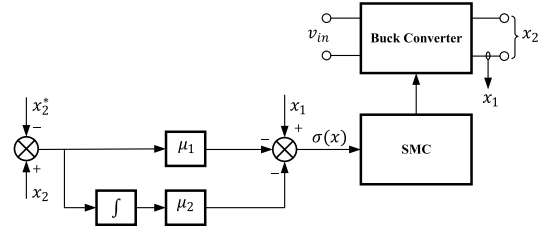


Fig. 7 Scheme for regulating the output voltage of the PV system.

5 Simulations and Results

In this section the results obtained for both the MPPT and voltage regulation of the PV system are presented. The simulations were performed using the Specialized Power Systems library of the MATLAB/Simulink software. The main characteristics under standard test conditions (STC) of the chosen PV module are shown in Table 1. The parameters of the converters used for MPPT and voltage regulation of the PV system are presented in Table 2.

5.1 Simulation Results for MPPT

The performance of the proposed APF-P&O algorithm is evaluated under different solar irradiation, and then comparisons are made with the conventional P&O method. In Figure 8, the results obtained for MPPT are presented, where the solar irradiation is 600 W/m^2 , from 0 to 1 second, then it reaches 800 W/m^2 from 1 to 2 seconds and 1000 W/m^2 from 2 to 3 seconds. As can be clearly seen from the graphs, the proposed APF-P&O method presents a better performance compared to the conventional P&O method. To demonstrate the effect of step size on the performance of the two algorithms, different step sizes were considered and the results obtained are shown in Figure 8. Compared to the conventional P&O method, it is possible to notice that the proposed method is less sensitive to step sizes, presents few ripples and rapidly converges to MPP.

5.2 Simulation Results for Voltage Regulation

Under the same solar irradiation conditions, the voltage regulation results are obtained. The reference voltage is assumed to be 32 V [1]. The output

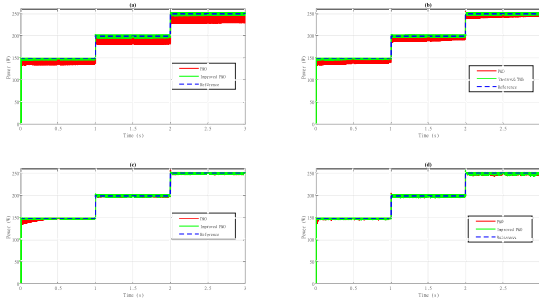


Fig. 8 Comparison between the proposed APF-P&O method and the conventional P&O: (a) MPPT for $\chi = 0.0001$; (b) MPPT for $\chi = 0.001$; (c) MPPT for $\chi = 0.01$; and (d) MPPT for $\chi = 0.1$.

voltage responses of the boost and buck converters are illustrated in Figures (9) and (10). The results show that although the input voltage of the buck converter varies due to changes in solar irradiation, its output voltage remains regulated.

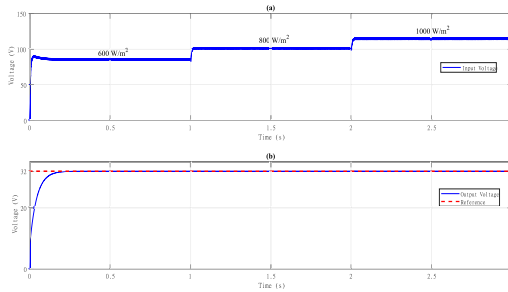


Fig. 9 Output voltages under increasing step-inputs of solar irradiation: (a) Boost converter output voltage; and (b) Buck converter output voltage (or PV system output voltage).

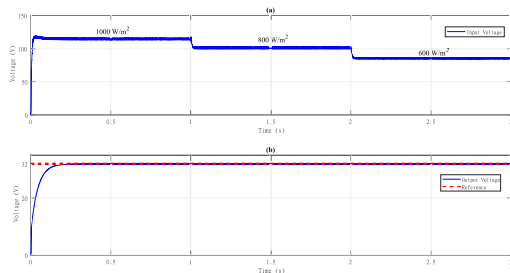


Fig. 10 Output voltages under decreasing step-inputs of solar irradiation: (a) Boost converter output voltage; and (b) Buck converter output voltage (or PV system output voltage).

Table 1 Key features of the TynSolar TYN-250P6 module under STC

Cells	
Technology	Polycrystalline silicon
Number of cells	66
Dimensions	156×156 mm
Structural Characteristics	
Dimensions L×W×H	1803×995×50 mm
Weight	22.0 kg
Electrical Characteristics	
Maximum power Pmax	250 W
Open circuit voltage Voc	40.06 V
Max. Power point voltage Vmpp	33.40 V
Short-circuit current Isc	8.10 A
Max. Power point current Impp	7.49 A

Table 2 Parameters of the DC-DC converters

Boost converter design parameters	
Input capacitance (C)	4 μ F
Inductance (L)	4.6 mH
Output capacitance (C)	181.85 μ F
Switching frequency (f_{sw})	10 kHz
Buck converter design parameters	
Inductance (L)	100 μ F
Capacitance (C)	10 μ F
Load (R)	60 Ω
Switching frequency (f_{sw})	10 kHz

6 Conclusions

This study presented a control strategy where both maximum power tracking and voltage regulation of a PV system are achieved simultaneously. A new method for MPPT inspired by artificial potential fields called APF-P&O is proposed and by means of comparisons with the conventional P&O method, its effectiveness is proven. The voltage obtained by the MPPT method is sent to the SMC which commands the boost input so that the MPP is reached. According to the simulations, the proposed APF-P&O method presents a relatively better performance in terms of convergence speed, sensitivity to step sizes, and output power ripples. For voltage regulation, another SMC with an appropriate control law is employed. Through simulations, it is verified that regardless of the variation of solar irradiation and the input voltage of the buck converter, the output voltage of the PV system remains regulated at the desired value. All simulations were performed using MATLAB/Simulink software. A recommendation for future research would be to add an anti-drifting feature to the proposed method.

References

- [1] M. Ma, X. Liu, and K. Y. Lee, “Maximum Power Point Tracking and Voltage Regulation of Two-Stage Grid-Tied PV System Based on Model Predictive Control,” *Energies*, vol. 13, no. 6, p. 1304, Mar. 2020, doi: 10.3390/en13061304.
- [2] A. K. Podder, N. K. Roy, and H. R. Pota, “MPPT methods for solar PV systems: a critical review based on tracking nature,” *IET Renew. Power Gener.*, vol. 13, no. 10, pp. 1615–1632, 2019.
- [3] M. Kermadi et al., “Recent developments of MPPT techniques for PV systems under partial shading conditions: a critical review and performance evaluation,” *IET Renew. Power Gener.*, 2020.
- [4] M. Sarvi and A. Azadian, “A comprehensive review and classified comparison of mppt algorithms in pv systems,” *Energy Syst.*, pp. 1–40, 2021.
- [5] S. B. R. Chowdhury, A. Mukherjee, and P. K. Gayen, “Maximum power point tracking of photovoltaic system by Perturb Observe and Incremental Conductance methods under normal and partial shading conditions,” in *2021 Innovations in Energy Management and Renewable Resources(52042)*, Feb. 2021, pp. 1–6, doi: 10.1109/IEMRE52042.2021.9386964.
- [6] Z. Kesilmiş, “A manhattan metric based perturb and observe maximum power point tracking algorithm for photovoltaic systems,” *Energy Sources, Part A Recover. Util. Environ. Eff.*, vol. 44, no. 1, pp. 469–492, Mar. 2022, doi: 10.1080/15567036.2022.2046662.
- [7] S. H. Sheikh Ahmadi, M. Karami, M. Gholami, and R. Mirzaei, “Improving MPPT Performance in PV Systems Based on Integrating the Incremental Conductance and Particle Swarm Optimization Methods,” *Iran. J. Sci. Technol. Trans. Electr. Eng.*, vol. 46, no. 1, pp. 27–39, Mar. 2022, doi: 10.1007/s40998-021-00459-0.
- [8] M. Elahi, H. M. Ashraf, and C.-H. Kim, “An Improved Partial Shading Detection Strategy Based on Chimp Optimization Algorithm to Find Global Maximum Power Point of Solar Array System,” *Energies*, vol. 15, no. 4, p. 1549, Feb. 2022, doi: 10.3390/en15041549.
- [9] S. N. Altamimi, E. A. Feilat, and D. A. Al Nadi, “Maximum Power Point Tracking Technique Using Combined Incremental Conductance and Owl Search Algorithm,” in *2021 12th International Renewable Engineering Conference (IREC)*, Apr. 2021, pp. 1–6, doi: 10.1109/IREC51415.2021.9427812.
- [10] A. A. Stephen, K. Musasa, and I. E. Davidson, “Modelling of Solar PV under Varying Condition with an Improved Incremental Conductance and Integral Regulator,” *Energies*, vol. 15, no. 7, p. 2405, Mar. 2022, doi: 10.3390/en15072405.
- [11] C. Pradhan, M. K. Senapati, N. K. Ntiakoh, and R. K. Calay, “Roach Infestation Optimization MPPT Algorithm for Solar Photovoltaic System,” *Electronics*, vol. 11, no. 6, p. 927, Mar. 2022, doi: 10.3390/electronics11060927.
- [12] M. N. Ali, K. Mahmoud, M. Lehtonen, and M. M. F. Darwish, “An Efficient Fuzzy-Logic Based Variable-Step Incremental Conductance MPPT Method for Grid-Connected PV Systems,” *IEEE Access*, vol. 9, pp. 26420–26430, 2021, doi: 10.1109/ACCESS.2021.3058052.
- [13] H.-H. Park and G.-H. Cho, “A DC–DC Converter for a Fully Integrated PID Compensator With a Single Capacitor,” *IEEE Trans. Circuits Syst. II Express Briefs*, vol. 61, no. 8, pp. 629–633, Aug. 2014, doi: 10.1109/TC-SII.2014.2327351.
- [14] G. Sulligoi, D. Bosich, G. Giadrossi, L. Zhu, M. Cupelli, and A. Monti, “Multiconverter Medium Voltage DC Power Systems on Ships: Constant-Power Loads Instability Solution Using Linearization via State Feedback Control,” *IEEE Trans. Smart Grid*, vol. 5, no. 5, pp. 2543–2552, Sep. 2014, doi: 10.1109/TSG.2014.2305904.
- [15] S. Jayaprakash and V. Ramakrishnan, “Analysis of solar based closed loop DC-DC converter using PID and fuzzy logic control for

- separately excited motor drive,” in 2014 IEEE National Conference on Emerging Trends In New & Renewable Energy Sources And Energy Management (NCET NRES EM), 2014, pp. 118–122, doi: 10.1109/NCETNRESEM.2014.708875.
- [16] Q. Wei, B. Wu, D. Xu, and N. R. Zargari, “Model Predictive Control of Capacitor Voltage Balancing for Cascaded Modular DC–DC Converters,” *IEEE Trans. Power Electron.*, vol. 32, no. 1, pp. 752–761, Jan. 2017, doi: 10.1109/TPEL.2016.2530869.
- [17] R. Ling, Z. Shu, Q. Hu, and Y.-D. Song, “Second-Order Sliding-Mode Controlled Three-Level Buck DC–DC Converters,” *IEEE Trans. Ind. Electron.*, vol. 65, no. 1, pp. 898–906, Jan. 2018, doi: 10.1109/TIE.2017.2750610.
- [18] V. Utkin, “Sliding mode control of DC/DC converters,” *J. Franklin Inst.*, vol. 350, no. 8, pp. 2146–2165, Oct. 2013, doi: 10.1016/j.jfranklin.2013.02.026.
- [19] M. C. Mira, A. Knott, O. C. Thomsen, and M. A. E. Andersen, “Boost converter with combined control loop for a stand-alone photovoltaic battery charge system,” in 2013 IEEE 14th Workshop on Control and Modeling for Power Electronics (COMPEL), Jun. 2013, pp. 1–8, doi: 10.1109/COMPEL.2013.6626428.
- [20] Y. Ravindranath Tagore, K. Rajani, and K. Anuradha, “Dynamic analysis of solar powered two-stage dc–dc converter with MPPT and voltage regulation,” *Int. J. Dyn. Control*, pp. 1–15, Apr. 2022, doi: 10.1007/s40435-022-00930-8.
- [21] S. A. Mohamed and M. Abd El Sattar, “A comparative study of PO and INC maximum power point tracking techniques for grid-connected PV systems,” *SN Appl. Sci.*, vol. 1, no. 2, p. 174, Feb. 2019, doi: 10.1007/s42452-018-0134-4.
- [22] A. Saidi and C. Benachaiba, “Comparison of IC and PO algorithms in MPPT for grid connected PV module,” in 2016 8th International Conference on Modelling, Identification and Control (ICMIC), Nov. 2016, pp. 213–218, doi: 10.1109/ICMIC.2016.7804300.
- [23] M. Kordestani, A. Mirzaee, A. A. Safavi, and M. Saif, “Maximum Power Point Tracker (MPPT) for Photovoltaic Power Systems-A Systematic Literature Review,” in 2018 European Control Conference (ECC), Jun. 2018, pp. 40–45, doi: 10.23919/ECC.2018.8550117.
- [24] M. Farhat, O. Barambones, and L. Sbita, “A new maximum power point method based on a sliding mode approach for solar energy harvesting,” *Appl. Energy*, vol. 185, pp. 1185–1198, Jan. 2017, doi: 10.1016/j.apenergy.2016.03.055.
- [25] H. U. Rahman Habib, S. Wang, M. F. Elmorsheedy, and A. Waqar, “Performance Analysis of Combined Model-Predictive and Slide-Mode Control for Power Converters in Renewable Energy Systems,” in 2019 22nd International Conference on Electrical Machines and Systems (ICEMS), Aug. 2019, pp. 1–5, doi: 10.1109/ICEMS.2019.8921860.
- [26] N. L. Manuel, N. İnanç, and M. Y. Erten, “Control of mobile robot formations using A-star algorithm and artificial potential fields,” *J. Mechatronics, Electr. Power, Veh. Technol.*, vol. 12, no. 2, pp. 57–67, Dec. 2021, doi: 10.14203/j.mev.2021.v12.57-67.
- [27] H. Komurcugil, S. Biricik, S. Bayhan, and Z. Zhang, “Sliding Mode Control: Overview of Its Applications in Power Converters,” *IEEE Ind. Electron. Mag.*, vol. 15, no. 1, pp. 40–49, Mar. 2021, doi: 10.1109/MIE.2020.2986165.
- [28] L. Wu, J. Liu, S. Vazquez, and S. K. Mazumder, “Sliding Mode Control in Power Converters and Drives: A Review,” *IEEE/CAA J. Autom. Sin.*, vol. 9, no. 3, pp. 392–406, Mar. 2022, doi: 10.1109/JAS.2021.1004380.
- [29] R. S. Inomoto, J. R. B. A. Monteiro, and A. J. Sguarezi Filho, “Boost Converter Control of PV System Using Sliding Mode Control With Integrative Sliding Surface,” *IEEE J. Emerg. Sel. Top. Power Electron.*, vol. 6777, no. c, pp. 1–1, 2022, doi: 10.1109/jestpe.2022.3158247.

- [30] A. Goudarzian, A. Khosravi, and H. A. Raeisi, “Optimized sliding mode current controller for power converters with non-minimum phase nature,” *J. Franklin Inst.*, vol. 356, no. 15, pp. 8569–8594, 2019, doi: 10.1016/j.jfranklin.2019.08.026.
- [31] H. Guldemir, “Study of Sliding Mode Control of Dc-Dc Buck Converter,” no. January 2011, 2015, doi: 10.4236/epe.2011.34051.